

A Patient-Derived Cellular Model for Huntington's Disease Reveals Phenotypes at Clinically Relevant CAG Lengths

Claudia L. Hung¹, Tamara Maiuri¹, Laura E. Bowie¹, Ryan Gotesman¹, Susie Son¹, Mina Falcone¹, James Giordano^{2,3}, Virginia Mattis⁴, Trevor Lau¹, Vickie Kwan^{1,5}, Vanessa C. Wheeler^{2,3}, Jonathan Schertzer¹, Karun Singh¹, *Ray Truant¹

¹Department of Biochemistry and Biomedical Sciences, Faculty of Health Sciences, McMaster University, Hamilton, ON, Canada

²Center for Genomic Medicine, Massachusetts General Hospital, Harvard Medical School, Boston, MA, United States

³Department of Neurology, Massachusetts General Hospital, Harvard Medical School, Boston, MA, United States

⁴Cedars-Sinai Medical Center, Board of Governors Regenerative Medicine Institute, Los Angeles, CA, United States

⁵Stem Cell and Cancer Research Institute, Faculty of Health Sciences, McMaster University, Hamilton, ON, Canada

*Corresponding Author: truantr@mcmaster.ca

ABSTRACT

The huntingtin protein participates in several cellular processes that are disrupted when the polyglutamine tract is expanded beyond a threshold of 37 CAG DNA repeats in Huntington's disease (HD). Cellular biology approaches to understand these functional disruptions in HD have primarily focused on cell lines with synthetically long CAG length alleles that clinically represent outliers in this disease and a more severe form of HD that lacks age-onset. Patient-derived fibroblasts are limited to a finite number of passages before succumbing to cellular senescence. We used human telomerase reverse transcriptase (hTERT) to immortalize fibroblasts taken from individuals of varying age, sex, disease onset and CAG repeat length, which we have termed TruHD cells. TruHD cells display classic HD phenotypes of altered morphology, size and growth rate, increased sensitivity to oxidative stress, aberrant ADP/ATP ratios and hypophosphorylated huntingtin protein. We additionally observed dysregulated ROS-dependent huntingtin localization to nuclear speckles in HD cells. We report the generation and characterization of a human, clinically relevant cellular model for investigating disease mechanisms in HD at the single cell level, which, unlike transformed cell lines, maintains TP53 function critical for huntingtin transcriptional regulation and genomic integrity.

INTRODUCTION

Huntington's disease (HD) is a late-onset, autosomal-dominant neurodegenerative disorder characterized by a triad of motor, cognitive and psychiatric symptoms. The disease is caused by a CAG trinucleotide expansion of >37 repeats in the huntingtin gene, manifesting as polyglutamine-expanded huntingtin protein¹. The functional implications of this expanded, mutant huntingtin are not fully understood. Much of the existing research on HD cell biology in relevant neuronal cell types has been limited to primary post-mitotic neurons from murine brain tissue or transformed cell lines, which have several limitations, including the use of synthetically long CAG lengths in order to mimic human disease in mice²⁻¹⁵. These alleles actually genetically model juvenile or Westphal variant HD, which are not age-onset diseases. The mean clinical CAG allele length is 43 repeats, with even >50 repeats representing statistical outliers¹⁶. Disease models in Neuro-2A cells, HEK293 or HeLa cells rely on cell transformation to maintain line longevity, but transformation typically involves initiating genomic instability and “shattering” of genomes^{17,18}, affecting intra- and inter-laboratory reproducibility.

The pursuit of investigating human cells has driven researchers to culture patient fibroblast cells that can be extracted from a skin biopsy¹⁹⁻²¹. Primary fibroblasts from HD patients possess clinically relevant polyglutamine expansion lengths, making them an attractive model for studying HD human cell biology. Further, they can be reprogrammed into induced pluripotent stem cells (iPSCs)²², which can be differentiated into various neuronal cell lineages²³⁻²⁵ or directly reprogrammed to medium spiny neurons²⁶⁻²⁹. However, primary fibroblasts are subject to telomere-controlled senescence, which limits the number of passages as telomeres shorten with each cell division^{30,31}. Senescent cells display altered gene expression, decreased proliferation and resistance to apoptotic mechanisms^{32,33}, hindering long-term use and consistency between trials.

We sought to overcome these limitations by immortalizing patient fibroblasts with human telomerase reverse transcriptase (hTERT). hTERT has been extensively used to immortalize human cell types to study cell biology in a number of diseases³⁴⁻³⁹. Like primary cells, hTERT-immortalized cells mimic *in vivo* tissue phenotypes⁴⁰, with the added benefits of proliferative capacity, karyotypic stability, and inter-experimental reproducibility⁴⁰.

We sought to generate a panel of human cell lines with polyglutamine expansions in the 40-50 CAG range, reflective of those seen in the clinic. We immortalized fibroblasts from 3 individuals and termed the cell lines TruHD cells: control female (TruHD-Q21Q18F), heterozygous male (TruHD-Q43Q17M), and homozygous female (TruHD-Q50Q40F) (Table 1). To validate these cells as HD models, we examined known model and patient phenotypes. Consistent with previous reports, we found that HD cells could be distinguished from wild type based on morphology^{7,15}, size¹⁵, growth rate^{20,41,42}, sensitivity to stress^{9,43-45}, aberrant ADP/ATP ratios^{7,46,47}, hypophosphorylated huntingtin protein⁴⁸⁻⁵⁰ and altered ROS-dependent localization to nuclear speckles⁵¹. We have therefore generated and characterized a panel of clinically relevant cellular models for investigating disease mechanisms in HD.

Genome-wide association studies (GWAS) in the HD research field revealed DNA damage and oxidative stress mechanisms as critical modifiers of the age of disease onset in patients⁵². One of the most important regulators of DNA repair, cell stress, and cell death responses is the TP53 protein⁵³⁻⁵⁵, which also directly regulates huntingtin transcription via a response element in the *HTT* promoter region^{56,57}. To date, the most widely used HD cell lines are SV40 large T-antigen-transformed mouse striatal cell lines (*STHdh*)⁷, which have become an invaluable tool for studying HD cell biology. However, conditional cell immortalization by transformation requires inhibited TP53 function. Investigation of the role of huntingtin in DNA damage and cell stress pathways may therefore be confounded by TP53 inactivation. In contrast, hTERT immortalization does not alter TP53 function^{35,58,59}, making TruHD cells an attractive model for these disease mechanisms in particular. Immortalized fibroblasts provide the added benefits of inter-experimental and inter-laboratory reproducibility, and long-term applications such as generation of stable cell lines and direct conversion to patient-specific human neurons. These cell models are readily available to the HD research community and will be freely distributed by our group.

RESULTS

Immortalization of Primary Fibroblasts with hTERT

Primary fibroblasts from various patients were obtained from the Coriell Institute for Medical Research and transduced with TERT Human Lentifact™ Purified Lentiviral Particles as described in methods. Three immortalized cell lines were generated from patients with varying CAG repeat lengths and disease onset age (Table 1) as representatives of control (TruHD-Q21Q18F), heterozygous HD (TruHD-Q43Q17M) and homozygous HD (TruHD-Q50Q40F). We standardized the line naming to a format compatible with digital file annotation, defining the CAG length of each *HTT* allele and the sex of the donor.

To verify that cells were successfully overexpressing hTERT, RNA levels in primary cells and TruHD cells were compared by quantitative PCR (qPCR), showing detectable hTERT mRNA levels in TruHD cells compared to primary cells normalized to commercially available hTERT-immortalized retinal pigment epithelial (RPE1) cells (Figure 1A). To ensure that the increased hTERT expression was associated with increased hTERT catalytic activity, telomerase activity was tested in TruHD-Q21Q18F and TruHD-Q43Q17M cells using a telomeric repeat amplification protocol (TRAP) assay. As shown in Figure 1B, multiple amplification products resulting from active hTERT were observed in TruHD cells, but not primary cells, indicating that the transduced hTERT is catalytically active in TruHD cells.

Unlike immortalization by transformation, hTERT immortalization maintains karyotypic stability in normal, human diploid cells^{35,38,58}. Chromosomal instability leading to polyploidy and aneuploidy can affect gene expression and cell viability, which is a hallmark of transformed cancer cells^{60,61}. To confirm karyotypic stability in TruHD cells after 25+ passages, we compared the karyotypes of *STHdh* cells and TruHD cells. Large chromosomal abnormalities were detected in transformed HD mouse striatal derived cells (*STHdh*^{Q111/Q111}) cells (Supplemental Figure 1A, Table 2), consistent with a recently published study¹⁵. No chromosomal changes were recorded for control TruHD-Q21Q18F, and minor chromosomal changes were recorded in TruHD-Q43Q17M and TruHD-Q50Q40F cell lines (Figure 1C, Table 2). In TruHD-Q43Q17M cells, the majority of the analyzed cells were missing one chromosome 16, and in TruHD-Q50Q40F cells, most of the cells

had an abnormal banding pattern on chromosome 4. These changes should be considered when interpreting results of phenotypic analysis.

Validation of CAG Repeats in TruHD Cell Lines

To verify that the CAG repeats of the fibroblasts matched the clinical information reported after successful immortalization, the CAG repeats were sized using a standardized *HTT* CAG repeat sizing assay^{62,63}. The length of each CAG tract was as expected (Table 3). The human huntingtin polyglutamine tract bears an additional CAACAG sequence beyond the pure CAG DNA tract sequence¹. These two additional codons encoding glutamine residues were not considered in the annotation by the Coriell Institute. Therefore, TruHD-Q21Q18F, for example, only refers to the polyglutamine tract that corresponds to the pure CAG tract, but the full polyglutamine tract lengths are actually Q23Q20. The true polyglutamine lengths corresponding to each TruHD cell line are listed in Table 3.

Defining Senescence in TruHD Cell Lines

Primary fibroblasts are typically cultured for approximately 15 passages from the initial skin biopsy before reaching senescence, while the successfully immortalized cells reported here can be passaged beyond 80 passages without reaching senescence (data not shown). Senescent cells show changes in cell growth, morphology and gene expression, which can be detected by an associated beta-galactosidase activity^{64,65}. Senescence was not detectable in TruHD immortalized cell lines (Supplemental Figure 1B) under normal culture conditions. We did note, however, that control TruHD-Q21Q18F fibroblasts seeded too sparsely exhibited senescence-associated beta-galactosidase activity (Supplemental Figure 1C) and stopped dividing. Normal, adherent cells in culture undergo contact inhibition, or post-confluence inhibition of cell mitosis^{64,66,67}. Essentially, once the cells become too confluent and make contact with nearby cells, they stop dividing and do not grow because of contact inhibition, unlike transformed cell lines. Cells that are left in this state for too long can become senescent and do not recover in culture⁶⁸. Specific protocols for freeze/thaw were therefore considered and explained in detail in the methods section. After 7 days of confluence without media changes, control cells were more susceptible to senescence compared

to the HD cell line (Supplemental Figure 1D). Upon karyotypic analysis of TruHD-Q21Q18F cells cultured under these conditions, a small percentage of control cells displayed tetraploidy (Supplemental Figure 1E), a phenomenon which has been reported to be a result of cellular senescence^{64,69}. In contrast, tetraploidy did not occur for either of the HD cell lines. Overall, we observed that cells did not senesce after extended passaging (over 80 passages), but control cells did senesce if cultured too sparsely or at high confluence, unlike HD cells which have a more senescence-resistant phenotype. This aspect of these cell lines could provide utility to study huntingtin biology in senescent cells, or cells in transition from mitotic to senescent.

Cell Morphology, Size, Growth and Viability

Mutant *STHdh* cells exhibit altered morphology^{7,15,44}. To probe whether TruHD cells could be distinguished by their morphology, nuclei were stained with Hoechst and immunofluorescence was performed with antibodies against phosphorylated huntingtin at serines 13 and 16 (N17-phospho) and beta-tubulin (Figure 2A). Images were analyzed with Phenoripper open software (www.phenoripper.org), which defines textures of the images in a non-supervised manner, and plots vectors of the three most variant textures in unitless 3D space using principal component analysis (PCA). This allows for identification of similarity between the images based on those defined features. Merged images of TruHD-Q21Q18F, TruHD-Q43Q17M and TruHD-Q50Q40F, considering the three parameters Hoechst, N17-phospho, and beta-tubulin, clustered apart from each other on a PCA plot (Figure 2B). The clustering pattern from each individual channel is shown in Supplemental Figure 2A, where beta-tubulin alone showed the greatest separation in the clusters compared to Hoechst and N17-phospho. This unbiased detection of a morphology phenotype between control and HD cells may be attributed to differences in cell size. We therefore compared cell size in control and mutant TruHD cells. Quantification of cell surface area shows that HD cells are smaller than control cells (Figure 2C). Therefore, consistent with numerous independent previous reports, huntingtin may be involved in cytoskeletal regulation^{15,70-72}.

Re-entry of post-mitotic neuronal cells into the cell cycle is a potential mechanism in the neurodegenerative process (see review⁷³). A consistent observation when culturing TruHD fibroblasts is that the mutant fibroblasts divide more rapidly, as seen with primary HD fibroblasts²⁰.

Monitoring proliferation of TruHD cells over 72 hours showed that TruHD-Q43Q17M cells double after ~20 hours, TruHD-Q50Q40F cells double after ~24 hours, while TruHD-Q21Q18F double after ~72 hours (Figure 2D). These observations are consistent with reports implicating huntingtin in cell cycle regulation and DNA damage repair mechanisms^{45,72,74} and that these functions are aberrant in HD cells.

Susceptibility to various types of cell stress is a well documented phenomenon in HD cellular models^{43,49,70,75}. We have previously shown that huntingtin responds to oxidizing agents by becoming phosphorylated, translocating from the ER to the nucleus and interacting with chromatin^{45,51}. We therefore tested TruHD cell viability upon oxidative stress with potassium bromate (KBrO₃) treatment over 24 hours. As shown in Figure 2E, both HD cell lines were most susceptible to cell death compared to the control line. Dose-dependent response of treatments in each individual TruHD cell line can be found in Supplemental Figure 2B.

Besides response to cell stress, another well documented HD phenotype is an energy deficit as measured by ADP/ATP ratio^{7,44,46}. The detection of ADP/ATP ratio in TruHD cells demonstrated an energy deficit in HD cell lines compared to the wild type cell line (Figure 2F) similar to the trend in *STHdh* cells (Supplemental Figure 2C), which is consistent with previously reported studies in HD models and synthetic allele lengths^{7,47}.

These phenotypes described in TruHD cells such as cell morphology, size, growth rate, susceptibility to oxidative stress and energy levels, demonstrate their utility as a cellular model with clinically relevant CAG allele lengths as phenotypes in mutant TruHD cells were all consistent with previous HD cellular models.

Total Huntingtin and Phosphorylated Huntingtin Protein Levels

Since the cells were taken from various patients and are not isogenic, the amount of total huntingtin was quantified. Validated antibodies to different epitopes of full-length huntingtin were used (EPR5526 and mAb2166), showing a minor decrease in total huntingtin levels in TruHD-Q50Q40F compared to TruHD-Q21Q18F and TruHD-Q43Q17M (Figure 3A, B).

Phosphorylation is a protective post-translational modification in HD cells⁴⁸⁻⁵⁰. Restoration of N17 phosphorylation is a therapeutic target in HD that has been explored by our lab and others

because mutant, polyglutamine-expanded huntingtin is hypophosphorylated at serines 13 and 16 (S13p and S16p respectively)⁴⁸⁻⁵⁰. Immunoblotting performed with a validated antibody against both serines (α -N17-phospho) (Supplemental Figure 3) showed decreased levels of N17 phosphorylation in mutant TruHD fibroblast cell lines compared to wild type (Figure 3C). Two distinct molecular weight bands are seen with the antibody, at ~350kDa and ~220kDa. Degradation products are often reported with other huntingtin antibodies as well, due to the large size of the protein and the rigorous processing steps of immunoblotting^{76,77}. Both bands were considered in quantifications, and this confirms hypophosphorylation of mutant huntingtin in a human HD. These results were verified by measuring whole-cell mean fluorescence intensity by flow cytometry (Figure 3D). Therefore, N17-phospho levels vary, but total huntingtin levels are invariant. This phenotype is consistent with previous reports⁴⁸⁻⁵⁰ and further validates N17-phosphorylation restoration as a target for HD therapeutic development.

Huntingtin Stress Response in Human Patient Fibroblasts

Huntingtin is a stress response protein and is involved in the unfolded protein response (UPR), DNA damage repair, oxidative stress and endoplasmic reticulum (ER) stress pathways^{43,45,51,78,79}. Previous studies from our lab show that huntingtin is bound to the ER membrane in steady state conditions and is released under conditions of stress, particularly ROS stress^{43,49}. Once soluble, huntingtin is phosphorylated at serines 13 and 16 (S13,S16), translocates to the nucleus and localizes to nuclear puncta^{49,51,80}. Using super-resolution structured-illumination microscopy (SR-SIM), we have now identified that these previously reported nuclear puncta are SC35 positive nuclear speckles: dynamic RNA/protein structures that are rich in mRNA splice factors that are important in cell stress responses⁸¹⁻⁸³ (Figure 4A).

We previously reported that stress-dependent phosphorylation of S13 and S16 promotes huntingtin localization to nuclear speckles in hTERT-immortalized human retinal pigment epithelial cells (RPE1)⁵¹. We therefore tested this phenomenon in TruHD cells. Cells were treated with 0.1mM 3-nitropropionic acid (3NP), a mitochondrial complex II inhibitor, for 1 hour to induce oxidative stress. We observed a significant increase in the number of nuclear speckles in TruHD-Q21Q18F cells (Figure 4B, C). However, in both the mutant TruHD-Q43Q17M and

TruHD-Q50Q40F lines, there was no significant difference in the number of nuclear speckles between treated and untreated conditions. The number of nuclear speckles in both heterozygote and homozygote HD cells were similar to that of TruHD-Q21Q18F in the presence of 3NP (N.S., $p=0.8475$), suggesting that in HD cells cells are under a chronic stress load.

Characterization of several HD phenotypes, combined with the establishment of methods to easily detect these disease-relevant phenotypes, in TruHD cells demonstrate their utility as a cellular model and will hopefully facilitate further investigation into pathological mechanisms.

DISCUSSION

Patient fibroblasts have been used previously by us and others^{19,41,42,45} to study HD cell biology, but currently there are no defined cell lines that are used consistently between projects. After generation of hTERT-immortalized TruHD cells, we focused on defining characteristics of these cells in order to facilitate their use. Our wild type line (TruHD-Q21Q18F), heterozygous HD line (TruHD-Q43Q17M) and homozygous HD line (TruHD-Q50Q40F) were chosen for this study as their CAG repeat lengths were most representative of annotated lengths, but also because they cultured well and the observed phenotypes were consistent throughout the study. A homozygote TruHD-Q50Q40F was chosen, because although a rare clinical example, this line could have utility as both alleles of huntingtin are mutant expanded, and thus can help resolve data in heterozygote lines, where mutant huntingtin phenotypes could be confounded by the presence of the normal allele.

We observed HD phenotypes in both heterozygous TruHD-Q43Q17M and homozygous TruHD-Q50Q40F cells, at clinically relevant CAG repeat lengths. Typical HD cell phenotypes include reduced cell size¹⁵, decreased cell viability upon cellular stress^{43,49,84}, altered cell proliferation¹⁵, decreased ADP/ATP ratio⁷ and hypophosphorylation of huntingtin N17 at serines 13 and 16⁴⁸⁻⁵⁰. Here, we have also demonstrated that HD cells showed altered susceptibility to cellular senescence and deficient response to oxidative stress as seen by SC35 nuclear speckle counts. Additionally, TruHD cells can be distinguished in an unbiased manner using non-supervised image texture analysis and principal component analysis via software such as Phenoripper. Phenoripper can be used as a readout for future high-content drug screening assays. Improvement in inter-experimental and inter-laboratory reproducibility have also been observed and may be beneficial for long-term applications such as generation of stable cell lines and cellular reprogramming to generate patient-specific neurons that maintain age-associated signatures^{26,28,29}.

Recent developments in understanding cell biology throughout the course of HD progression highlight the need for improved methods for disease modelling. DNA damage repair pathways have been implicated as the predominant modifiers of HD pathogenesis⁵². Previous observations in our lab show that huntingtin can sense oxidative stress and that huntingtin is involved in the DNA damage response⁴⁵. These processes require TP53 which an important

transcription factor that integrates various cellular stress signals and is widely considered the master regulator of genomic integrity due to its roles in DNA damage sensing, cell cycle checkpoint control and apoptotic regulation (see reviews⁸⁵⁻⁸⁷).

The choice of model system for studying certain aspects of cell biology is therefore critical. Historically, synthetically long CAG repeat alleles of *HTT* have been used in cell models because of the apparent lack of obvious phenotypes of clinical HD alleles in animal models. Cell biology research in HD has been primarily focused on neurons from HD mouse models and easily accessible cell lines, each with their own restrictions and limitations. The main limitation of cells taken from mouse models are the synthetically long polyglutamine tracts used in order to mimic a late-onset human disease within the lifespan of a mouse. In these models, it can be overlooked that the majority of patients have CAG repeats between 40-50, and that these patients have varying age onset that is not attributed to just the number of repeats. Additionally, some models are transgenic, and thus do not have an accurate gene dosage, while others express huntingtin at super-physiological levels, confounding data with incorrect protein stoichiometry, which can be a concern for a scaffolding protein. This is the first characterized human HD immortalized cell line model and can therefore be used to test therapeutic reagents that are designed specifically for human cells and will be a tool for the HD research community.

METHODS

Cell Culture and Generation of hTERT-Immortalized Fibroblasts

Patient fibroblasts were purchased from the Coriell Institute from the NINDS repository. HD patient fibroblasts (ND30013, GM04857) and control patient fibroblasts (ND30014) were obtained. Cells were cultured in Minimum Essential Media (MEM, Gibco #10370) with 15% fetal bovine serum (FBS, Gibco) and 1X GlutaMAX (Gibco #35050). Cells were infected with 1×10^6 TERT Human Lentitect™ Purified Lentiviral Particles (GeneCopoeia, LPP-Q0450-Lv05-200-S). To aid in infection, 10 µg/mL polybrene was added. After 8 hours, cells were infected again and left for 24 hours. Media was changed and cells were left for an additional 48 hours. Successfully transduced cells were selected in media with 1 µg/mL puromycin. Cells were grown at 37°C with 5% CO₂.

STHdh cells (a kind gift from Dr. Marcy Macdonald) were cultured in Dulbecco's Modified Eagle Medium (DMEM, Gibco #11995) with 10% FBS. Cells were grown at 33°C with 5% CO₂. RPE1 cells (ATCC) were cultured in 1:1 Dulbecco's Modified Eagle Medium/Nutrient Mixture F-12 (DMEM/F12, Gibco #11330) with 10% FBS and 0.01% hygromycin. Cells were grown at 37°C with 5% CO₂.

Quantitative PCR to Measure hTERT mRNA Levels

Primary, TruHD and RPE1 cells were grown to ~85% confluence. Total RNA was obtained from frozen cell pellets lysed in 1 mL of Trizol (Thermo Fisher Scientific) per $\sim 1 \times 10^6$ cells, followed by phenol-chloroform extraction. RNA was treated with DNase I (Thermo Fisher Scientific) and cDNA was prepared using 1000 ng total RNA and SuperScript III Reverse Transcriptase (Thermo Fisher Scientific). Transcript expression was measured using TaqMan Assays with AmpliTaq Gold DNA polymerase (Thermo Fisher Scientific), and *hTERT* (Hs00972650_m1) was compared to *ACTB* (Hs01060665_g1) housekeeping gene using the $\Delta\Delta C_T$ method.

Telomeric Repeat Amplification Protocol

Primary fibroblasts and corresponding TruHD cells were grown to ~85% confluence. A two-step PCR method (TRAPeze® Telomerase Detection Kit S7700, Millipore) was used to evaluate hTERT catalytic activity. Briefly, in the first step, telomerases from lysed cells add telomeric repeats (AG followed by repetitive GGTTAG sequences) on the 3' end of a substrate oligonucleotide (TS). In the second step, the extended products are amplified by PCR using a primer specific for the beginning of TS, and a reverse primer specific for the end of the repeats. The lowest amplification product should be 50 bp, and increases by 6 bp-long repeat increments are visualized, on a 10% TBE polyacrylamide gel.

Cryogenic Storage of TruHD Cells

For freezing one vial of TruHD cells, a plate was grown to 90% confluence (~1 x 10⁵/mL) on a 10 cm dish and was split in half. The next day, two ~60% confluent plates, that were still in growth phase, were trypsinized and combined. Cells were centrifuged at 1500 rpm and pellets were resuspended in culture media with 1 mL of 5% DMSO. Vials were put into a slow-freeze unit in the -80°C to ensure optimal cell preservation. After 24-48 hours, vials were moved to a -150°C for long-term storage.

Vials were thawed slowly at 37°C for around 2-5 minutes. Using a 10 mL pipette, the 1 mL of cells were moved directly into a 10 cm plate already pre-incubated with media. After 24 hours, media was changed to remove residual DMSO.

Sizing of CAG Repeat

TruHD cells were grown to ~90% confluence in a 10 cm plate. Cells were scraped and centrifuged at 4°C at 1500 rpm. Genomic DNA was extracted using the PureLink® Genomic DNA kit (ThermoFisher). A fluorescence-based assay was used to size the CAG repeats, based on the originally described assay by Warner et al.⁶³ and further described in Keum et al.⁶²

Karyotyping

Karyotyping was performed by The Centre for Applied Genomics, The Hospital for Sick Children, Toronto, Canada. Karyotype analysis via G-banding was performed on cells from two

T25 flasks per cell line. When cells reached 80-90% confluence, Karyomax Colcemid[®] was added to each flask to a final concentration of 0.1 µg/mL (Gibco #15212-012) and incubated in 37°C CO₂ incubator for 1.5-2 hours (for TruHD-Q43Q17M and TruHD-Q50Q40F) and 3-4 hours for TruHD-Q21Q18F. Cells were then collected and suspended in 6 mL of 0.075 M KCl, and incubated at 37°C for 20 minutes. Eight drops of Carnoy's Fixative (methanol/acetic acid, 3:1) was added and mixed together. The cells were centrifuged at 1000 rpm for 10 minutes at room temperature and cell pellets were collected. After three rounds of fixations (add 8 mL fixative and centrifuge at 1000 rpm for 10 minutes), cells were resuspended in 0.5-1 mL of fixative and cells from each suspension were dispensed onto glass slides and baked at 90°C for 1.5 hours. Routine G-banding analysis was then carried out. Approximately 15-20 metaphases per cell line were examined.

Senescence-Associated Beta-Galactosidase Activity Assay

TruHD and primary fibroblasts were seeded into a 6 well plate. Primary fibroblasts reached ~20 passages before analysis and TruHD cells reached ~50 passages. When cells reached ~90% confluency, media was aspirated and cells were washed 1X with PBS and experiments were carried out using Senescence Detection Kit (Abcam, ab65351) manufacturer instructions.

Phenoripper and Cell Surface Area Measurement

Immunofluorescence was performed with Hoechst 33342 (ThermoFisher), beta-tubulin antibody (E7, DSHB, 1:250 dilution in 2% FBS in PBS with 0.02% Tween) and N17-phospho antibody (NEP, see section on antibody validation) were analyzed using Phenoripper. Five images per trial of TruHD fibroblasts acquired on a Nikon TiEclipse inverted epifluorescent widefield using a 20X objective (NA=0.75) and Spectra X LED lamp (Lumencor) capture using an Orca-Flash 4.0 CMOS camera (Hamamatsu). Cell surface area was calculated with ImageJ. Cells were thresholded to remove background to identify whole-cell region of interest and area of each cell was measured and plotted.

Cell Counting

Cells were seeded into a 24 well plate (10^5 /mL). After 24 hours, nuclei were stained for 15 minutes with NucBlue Live ReadyProbes Reagent (1 drop/mL of media) (ThermoFisher). Cells were imaged using the Nikon TiEclipse inverted widefield epifluorescent microscope, and using an automated round object detector in NIS Elements Advanced Research 4.30.02v software (Nikon), cell nuclei were counted. This was repeated repeat plates that were left for 48 and 72 hours for all cell lines.

ADP/ATP Ratio Assay

ADP/ATP Ratio Assay Kit (Sigma MAK135) was used according to the protocol, except the first step to seed TruHD cells directly into a 96 well plate which the rest of the assay is performed on. If seeded directly into a 96 well plate, there is not enough room to grow the suggested 10^4 fibroblast cells because of their large size. Therefore, TruHD cells were seeded into a 24 well plate, for no more than 48 hours, to ~80% confluency. After reaching confluency, the cells are lysed with the working reagent (provided in the kit). After lysing, cells from the 24 well plate were moved directly into a 96 well plate to continue the rest of the assay according to the protocol. For *STHdh* cells, assay was performed according to the protocol with no changes.

Cell Viability Assay

Cells were seeded into a 96 well plate. After 24 hours, cells were stained for 15 minutes with NucBlue Live ReadyProbes Reagent (1 drop/mL of media) (ThermoFisher) in Hank's Balanced Salt Solution (HBSS) (Gibco). Cells were washed with once with HBSS and treated with 100 μ L of potassium Bromate (KBrO_3) (Millipore) at concentrations of 0, 1, 10, 100 and 200 mM in HBSS with NucGreen Dead 488 ReadyProbes Reagent (1 drop/mL of media) (ThermoFisher).

The 96 well plate was imaged immediately over the course of 24 hours every 20 minutes at 37°C using a Nikon TiEclipse inverted A1 confocal microscope equipped with a 20X objective (NA= 0.75) and driven by NIS Elements AR 4.30.02v 64-bit acquisition software (Nikon). Cells were imaged simultaneously in the FITC (NucGreen) and DAPI (NucBlue) channels. A cell was defined as undergoing cell death when 50% or more of the nucleus, as defined by NucBlue-positive

pixels, was overlapped by NucGreen-positive pixels. Cell death was multiplied by 100% and subtracted from 100 to calculate % Viability. Images were analyzed using Python.

Immunoblotting

TruHD cells were grown to ~90% confluence. Cells were scraped and centrifuged at 4°C at 1500 rpm. Cell pellets were lysed in radioimmunoprecipitation assay (RIPA) buffer with 10% phosphatase (Roche) and 10% protease inhibitors (Roche) for 12 minutes on ice and centrifuged at 10 000 x g at 4°C for 12 minutes. Supernatant was collected and 40 µg of protein was loaded into a pre-cast 4-20% polyacrylamide gradient gel (Biorad). Proteins were separated by SDS-PAGE and electroblotted onto 0.45 µm poly-vinyl difluoride (PVDF) membrane (EMD Millipore).

Blots were blocked with 5% non-fat dry milk in TBS-T (50 mM Tris-HCl, pH 7.5, 150 mM NaCl, 0.1% Tween-20) for 1 hour at room temperature. Blots were then incubated with primary N17-phospho antibody (1:1250), EPR5526 (1:2500, Abcam ab106115), mAb2166 (1:2500, Millipore) or GAPDH (1:10 000, Abcam ab8425) overnight at 4°C. Blots were washed 3 times for 10 minutes with TBS-T and then incubated with anti-rabbit or anti-mouse HRP secondary (1:50 000, Abcam) for 45 minutes at room temperature. Finally, blots were washed 3 times for 10 minutes with TBS-T and visualized with enhanced chemiluminescent HRP substrate (EMD Millipore) on a MicroChemi system (DNR Bio-imaging Systems). Huntingtin bands were quantified using NIH ImageJ and normalized to the GAPDH loading control.

Flow Cytometry

TruHD cells were grown to ~90% confluence. Cells were scraped and centrifuged at 4°C at 1500 rpm. Cells (~10⁶) were resuspended and fixed in ice-cold methanol for 12 minutes, inverting every 4 minutes. Cells were centrifuged at 4°C at 10 000 x g for 5 minutes followed by 2 washes in flow buffer (PBS with 2.5 mM EDTA and 0.5% BSA), and blocked in flow buffer with 2% FBS for 1 hour at room temperature. Cells were incubated overnight in AlexaFluor488-conjugated N17-phospho antibody, diluted 1:15 in flow buffer with 0.02% Tween-20, rotating at 4°C. Cells were washed twice and resuspended in flow buffer.

3NP Treatment and Nuclear Speckle Count

TruHD cells were treated with 0.1 mM 3-nitropropionic acid (3NP) for 1 hour at 37°C, then fixed and permeabilized with ice-cold methanol for 12 min. Cells were washed in PBS and blocked in antibody solution (2% FBS, 0.1% (v/v) Triton X-100 in 1X TBS) at room temperature for 10 minutes. AlexaFluor488-conjugated N17-phospho antibody was diluted 1:15 in antibody solution and incubated overnight at 4°C. Cells were washed in PBS and stained with Hoechst 33342 dye for 12 minutes at room temperature and left in PBS prior to imaging.

Cells were imaged using Nikon TiEclipse inverted widefield epifluorescent microscope using a Plan Apo 60X (NA=1.4) oil objective and Spectra X LED lamp (Lumencor) captured on an Orca-Flash 4.0 CMOS camera (Hamamatsu). A z-stack was obtained for each image and displayed as a maximum projection prior to image analysis. Image acquisition was completed using the NIS-Elements Advanced Research 4.30.02v 64-bit acquisition software (Nikon). Nuclear speckles were quantified in over 200 cells over 3 trials using an open source speckle counting pipeline in CellProfiler (www.cellprofiler.org).

Dot Blot Assay for Antibody Validation

Varying concentrations (from 25-1000 ng) of different synthetic N17 peptides (N17, N17S13p, N17S16p, and N17S13pS16p) were spotted onto a nitrocellulose membrane (Pall Life Sciences) and allowed to dry at room temperature for 45 minutes. Immunoblotting was carried out as described earlier.

Immunofluorescence Peptide Competition Assay for Antibody Validation

The N17-phospho antibody (1:250) was incubated, with rotation, with 1000 ng of synthetic N17 peptides (N17, N17S13p, N17S16p, N17S13pS16p, and a control peptide – p53 (371-393); New England Peptides) at room temperature for 1 hour prior to overnight incubation with RPE1 cells fixed with methanol. Cells were washed 3 times with 2% FBS in PBS and then incubated in anti-rabbit AlexaFluor488 secondary antibody (1:500, Molecular Probes) for 45 minutes at room temperature and then washed and left in PBS before imaging using a Nikon TiEclipse inverted epifluorescent microscope.

Huntingtin siRNA Knockdown for Antibody Validation

Endogenous huntingtin knockdown was established with huntingtin siRNA (Santa Cruz, sc35617) in RPE1 cells. siRNA was transfected using Lipofectamine RNAiMax (Invitrogen) according to manufacturer instructions. Control dishes were transfected with scrambled siRNA. Protein was extracted using as described earlier, and 60 μ g protein was loaded. Immunoblotting was carried out as described earlier.

Statistics

Data with a normal distribution were analyzed by unpaired t-test unless otherwise stated. Error bars represent standard error of the mean (S.E.M.).

Data Availability

The raw datasets generated and analyzed for this study are available from the corresponding author on reasonable request.

ACKNOWLEDGEMENTS

The authors wish to thank Raymond Wong of The Centre for Applied Genomics, The Hospital for Sick Children, Toronto, Canada for assistance with G-banding karyotype analysis and Alina Lelic of the Human Immune Testing Suite, McMaster Immunology Research Centre, Hamilton, Canada for assistance with flow cytometry experiments. This work was supported by the Canadian Institutes Of Health Research, grant MOP-119391, the Krembil Foundation and the Huntington Society of Canada.

AUTHOR CONTRIBUTIONS

C.L.K. and R.T. created experiments. C.L.K. wrote manuscript. T.M. and R.T. helped with editing. M.F. provided technical assistance. C.L.K. performed all experiments except for the following: V.M. and V.K. transduced patient cell lines for immortalization. J.G. and V.C.W. performed CAG repeat sizing. T.L. performed qPCR. L.E.B performed antibody validation experiments. R.G. performed cell viability experiments. S.S. performed nuclear speckle count. T.M. performed super-resolution imaging of nuclear speckles.

CONFLICTS OF INTEREST

The authors declare that there are no conflicts of interest.

FIGURE CAPTIONS

Figure 1: Generation of TruHD immortalized cell lines. (A) hTERT mRNA levels normalized to beta-actin (β -actin) mRNA levels in RPE1 cells (positive control), primary cells and TruHD cells. hTERT levels in primary cells were not detectable (N.D.). $n=5$. Error bars represent S.E.M. $*p=0.0369$ comparing TruHD-Q21Q18F, TruHD-Q43Q17M and TruHD-Q50Q40F by one-way ANOVA. (B) Telomeric repeat amplification product (TRAP) assay. Amplification products run on 10% TBE gel after telomere extension reaction, showing telomeric repeats >50 bp in increments of 6 bp. Template strand is 36 bp. Negative control contains no Taq polymerase or template strand. (C) Representative karyotypes of TruHD-Q21Q18F, TruHD-Q43Q17M and TruHD-Q50Q40F cells. “mar” denotes marker chromosomes, “+” are additional chromosomes and “?add(4)(p14)” denotes additional patterns observed on chromosome 4 at band p14. Results from full karyotype shown in Table 2.

Figure 2: TruHD cell properties. (A) Immunofluorescence images of TruHD-Q21Q18F, TruHD-Q43Q17M and TruHD-Q50Q40F. Scale bar = $10\mu\text{m}$. (B) PCA plot of images sorted with Phenoripper. (C) Cell surface area comparison in TruHD cells. $n=3$, $N>200$. Error bars represent S.E.M. $*p<0.0001$. (D) Relative cell count measured every 24 hours. $n=3$, $N>200$. Error bars represent S.E.M. $***p=0.0003$ at 48 hours, $***p=0.0001$ at 72 hours by one-way ANOVA. (E) Percent cell viability of TruHD cells compared to *STHdh* cells. $n=3$, $N>200$. Error bars represent S.E.M. At 24 hours, $****p<0.0001$ for *STHdh*^{Q7/Q7} vs *STHdh*^{Q111/Q111} by two-ANOVA and $****p<0.0001$ for TruHD-Q21Q18F vs TruHD-Q43Q17M and TruHD-Q50Q40F by two-way ANOVA. (F) Normalized ADP/ATP ratio in TruHD cells at $\sim 75\%$ confluency 24 hours after seeding. $n=3$, $N>200$. Error bars represent S.E.M. $*p=0.0371$ and $**p=0.0048$.

Figure 3: Huntingtin protein levels in TruHD cells. (A) Densitometric analysis of total huntingtin levels using western blot with EPR5526 antibody. Normalized to control TruHD-Q21Q18F cells. n=6. Error bars represent S.E.M. **p=0.0087 and *p=0.0254 by unpaired t-test. (B) Densitometric analysis of total huntingtin levels using western blot with mAb2166 antibody. Normalized to control TruHD-Q21Q18F cells. n=4. Error bars represent S.E.M. (C) Densitometric analysis of N17-phospho levels using western blot. Normalized to control TruHD-Q21Q18F cells. n=4. Error bars represent S.E.M. **p=0.0020 by unpaired t-test. (D) Mean fluorescence intensity analysis of N17-phospho using flow cytometry. Normalized to control TruHD-Q21Q18F. n=4. Error bars represent S.E.M. ***p=0.0005, *p=0.0159 and ****p<0.0001 by unpaired t-test.

Figure 4: Huntingtin localizes to nuclear speckles in response to stress. (A) N17-phospho localizes to SC35+ nuclear speckles. (B) Nuclear speckles are increased in TruHD-Q21Q18F control cells upon treatment with 0.1mM 3NP, but not for TruHD-Q43Q17M or TruHD-Q50Q40F. Scale bar =10µm. (C) Quantification of nuclear speckles. n=3, N=180. Error bars represent S.E.M. ****p<0.0001 by unpaired t-test. Comparison of TruHD-Q21Q18F 3NP, TruHD-Q43Q17M CTRL, TruHD-Q43Q17M 3NP, TruHD-Q50Q40F CTRL and TruHD-Q50Q40F 3NP by one-way ANOVA shows no significant difference (p=0.8475).

Supplemental Figure 1: (A) *STHdh*^{Q111/Q111} example karyotype. “mar” denotes marker chromosomes, “+” are additional chromosomes and “-” are missing chromosomes. (B) Senescence-activated beta-galactosidase assay comparing primary-Q21Q18F and TruHD-Q21Q18F cells at ~80% confluency. Senescent cells present blue colour pseudocoloured in greyscale and indicated by black arrow. Scale bar =250µm. (C) TruHD-Q21Q18F plated at lower density (<40% confluency) showed presence of blue colour pseudocoloured in greyscale and indicated by black arrow. Scale bar =250µm. (D) TruHD-Q21Q18F cells at high density that were left to overgrow (100% confluency) showed presence of blue colour pseudocoloured in greyscale and indicated by black arrow, but not as much in TruHD-Q43Q17M. Scale bar =250µm. (E) TruHD-Q21Q18F karyotype of senescent cells showing tetraploidy in 2 of 22 cells analyzed.

Supplemental Figure 2: (A) Individual PCA plots from Phenoripper comparing images of TruHD cell lines using only Hoechst (405nm), N17-phospho (488nm) and beta-tubulin (640nm) channels. (B) Dose response curves of TruHD cell lines to KBrO_3 . $n=3$, $N>200$. Error bars represent S.E.M. At 24 hours, **** $p<0.0001$ between 0mM and 10mM treatments in TruHD-Q43Q17M and TruHD-Q50Q40F cells by two-way ANOVA. (C) Normalized ADP/ATP ratio in *STHdh* cells at ~75 percent confluency 24 hours after seeding. $n=3$. Error bars represent S.E.M. ** $p=0.0014$.

Supplemental Figure 3: N17-phospho antibody validation (A) Dot blot with N17 peptides. Unphosphorylated (N17), phosphorylated on serine 13 only (N17 S13p), phosphorylated on serine 16 only (N17 S16p) and phosphorylated on both serines 13 and 16 (N17 S13pS16p). (B) Huntingtin knock-down showing N17-phospho antibody specificity compared to the commercially available total huntingtin antibody EPR5526. ** $p=0.0035$ for N17-phospho and ** $p=0.0031$ for EPR5526. (C) Peptide competition assay with N17 peptides and non-specific TP53 peptide. Scale bar = 20 μm .

TABLES

Table 1: TruHD Patient Fibroblast Information

Primary Cell Name	Cell Line Name	Allele 1	Allele 2	Sex	Age at Sampling	Disease Onset Age
ND30013	TruHD-Q43Q17M	43 CAG	17 CAG	Male	54	50
ND30014	TruHD-Q21Q18F	21 CAG	18 CAG	Female	52	-
GM04857	TruHD-Q50Q40F	50 CAG	40 CAG	Female	23	28

Table 2: G-band Karyotyping

[] = number of analyzed cells with specified karyotype

Cell Line	Karyotype (bold = representative result)
TruHD-Q21Q18F	46,XX[13] , 92,XXXX[2]
TruHD-Q43Q17M	46,XY,-16,+mar[9] , 47,XY,+7[3], 46,XY[3]
TruHD-Q50Q40F	46,XX,?add(4)(p14)[9]
<i>STHdh</i> ^{Q111/Q111}	70-82<4n>, XX or XXX or XXXX, -X[12], -X[4],add(X)(F1)[2],-1[9],add(1)(F)[3],del(1)(?G)[3],+2[2],-2[7],-4[7],?add(4)(C4)[3],dic(4;?)(?D;?)[2],+5[3],-6[8],-7[19],-7[5],+8[4],-8[4],rob(8;8)(A1;A1)[2],-9[12]+11[4],-11[3],-12[19],-12[6],-13[6],-14[15],-14[6],+15[18],+15[15],+15[4],-17[11],-17[3],-18[15],-18[3],+19[17],+1-15mar[20][cp20]

Table 3: Sizing of CAG and CCG repeats in TruHD Fibroblasts

Cell Line Name	CAGn Repeats	Q lengths (= CAG +2, based on genetic structure of CAGnCAACAG in humans)
TruHD-Q21Q18F	21 CAG/18 CAG	23Q/20Q

TruHD-Q43Q17M	43 CAG/17 CAG	45Q/19Q
TruHD-Q50Q40F	50 CAG/40 CAG	52Q/42Q

REFERENCES

1. A novel gene containing a trinucleotide repeat that is expanded and unstable on Huntington's disease chromosomes. The Huntington's Disease Collaborative Research Group. *Cell* **72**, 971–983 (1993).
2. Hodgson, J. G. *et al.* A YAC mouse model for Huntington's disease with full-length mutant huntingtin, cytoplasmic toxicity, and selective striatal neurodegeneration. *Neuron* **23**, 181–192 (1999).
3. Mangiarini, L. *et al.* Exon 1 of the HD gene with an expanded CAG repeat is sufficient to cause a progressive neurological phenotype in transgenic mice. *Cell* **87**, 493–506 (1996).
4. Schilling, G. *et al.* Intranuclear inclusions and neuritic aggregates in transgenic mice expressing a mutant N-terminal fragment of huntingtin. *Hum. Mol. Genet.* **8**, 397–407 (1999).
5. Shelbourne, P. F. *et al.* A Huntington's disease CAG expansion at the murine Hdh locus is unstable and associated with behavioural abnormalities in mice. *Hum. Mol. Genet.* **8**, 763–774 (1999).
6. Lin, C. H. *et al.* Neurological abnormalities in a knock-in mouse model of Huntington's disease. *Hum. Mol. Genet.* **10**, 137–144 (2001).
7. Trettel, F. *et al.* Dominant phenotypes produced by the HD mutation in STHdh(Q111) striatal cells. *Hum. Mol. Genet.* **9**, 2799–2809 (2000).

8. Wytenbach, A. *et al.* Polyglutamine expansions cause decreased CRE-mediated transcription and early gene expression changes prior to cell death in an inducible cell model of Huntington's disease. *Hum. Mol. Genet.* **10**, 1829–1845 (2001).
9. Slow, E. J. *et al.* Selective striatal neuronal loss in a YAC128 mouse model of Huntington disease. *Hum. Mol. Genet.* **12**, 1555–1567 (2003).
10. Menalled, L. B., Sison, J. D., Dragatsis, I., Zeitlin, S. & Chesselet, M.-F. Time course of early motor and neuropathological anomalies in a knock-in mouse model of Huntington's disease with 140 CAG repeats. *J. Comp. Neurol.* **465**, 11–26 (2003).
11. Gray, M. *et al.* Full-length human mutant huntingtin with a stable polyglutamine repeat can elicit progressive and selective neuropathogenesis in BACHD mice. *J. Neurosci.* **28**, 6182–6195 (2008).
12. Menalled, L. B. *et al.* Comprehensive behavioral and molecular characterization of a new knock-in mouse model of Huntington's disease: zQ175. *PLoS One* **7**, e49838 (2012).
13. Ferris, C. F. *et al.* Studies on the Q175 Knock-in Model of Huntington's Disease Using Functional Imaging in Awake Mice: Evidence of Olfactory Dysfunction. *Front. Neurol.* **5**, 94 (2014).
14. Southwell, A. L. *et al.* An enhanced Q175 knock-in mouse model of Huntington disease with higher mutant huntingtin levels and accelerated disease phenotypes. *Hum. Mol. Genet.* **25**, 3654–3675 (2016).
15. Singer, E. *et al.* Reduced cell size, chromosomal aberration and altered proliferation rates are characteristics and confounding factors in the STHdh cell model of Huntington disease. *Sci. Rep.* **7**, 16880 (2017).

16. Myers, R. H. Huntington's disease genetics. *NeuroRx* **1**, 255–262 (2004).
17. Landry, J. J. M. *et al.* The genomic and transcriptomic landscape of a HeLa cell line. *G3* **3**, 1213–1224 (2013).
18. Mittelman, D. & Wilson, J. H. The fractured genome of HeLa cells. *Genome Biol.* **14**, 111 (2013).
19. Barkley, D. S., Hardiwidjaja, S. & Menkes, J. H. Abnormalities in growth of skin fibroblasts of patients with Huntington's disease. *Ann. Neurol.* **1**, 426–430 (1977).
20. Goetz, I. E., Roberts, E. & Warren, J. Skin fibroblasts in Huntington disease. *Am. J. Hum. Genet.* **33**, 187–196 (1981).
21. del Hoyo, P. *et al.* Oxidative stress in skin fibroblasts cultures of patients with Huntington's disease. *Neurochem. Res.* **31**, 1103–1109 (2006).
22. HD iPSC Consortium. Induced pluripotent stem cells from patients with Huntington's disease show CAG-repeat-expansion-associated phenotypes. *Cell Stem Cell* **11**, 264–278 (2012).
23. Juopperi, T. A. *et al.* Astrocytes generated from patient induced pluripotent stem cells recapitulate features of Huntington's disease patient cells. *Mol. Brain* **5**, 17 (2012).
24. Martinez, Y., Dubois-Dauphin, M. & Krause, K.-H. Generation and applications of human pluripotent stem cells induced into neural lineages and neural tissues. *Front. Physiol.* **3**, 47 (2012).
25. Zhang, Y. *et al.* Rapid single-step induction of functional neurons from human pluripotent stem cells. *Neuron* **78**, 785–798 (2013).
26. Yoo, A. S. *et al.* MicroRNA-mediated conversion of human fibroblasts to neurons. *Nature* **476**, 228–231 (2011).

27. Xue, Y. *et al.* Direct conversion of fibroblasts to neurons by reprogramming PTB-regulated microRNA circuits. *Cell* **152**, 82–96 (2013).
28. Victor, M. B. *et al.* Generation of human striatal neurons by microRNA-dependent direct conversion of fibroblasts. *Neuron* **84**, 311–323 (2014).
29. Victor, M. B. *et al.* Striatal neurons directly converted from Huntington’s disease patient fibroblasts recapitulate age-associated disease phenotypes. *Nat. Neurosci.* (2018).
doi:10.1038/s41593-018-0075-7
30. Hayflick, L. & Moorhead, P. S. The serial cultivation of human diploid cell strains. *Exp. Cell Res.* **25**, 585–621 (1961).
31. Hayflick, L. The limited in vitro lifetime of human diploid cell strains. *Exp. Cell Res.* **37**, 614–636 (1965).
32. Dimri, G. P. *et al.* A biomarker that identifies senescent human cells in culture and in aging skin in vivo. *Proc. Natl. Acad. Sci. U. S. A.* **92**, 9363–9367 (1995).
33. Marcotte, R., Lacelle, C. & Wang, E. Senescent fibroblasts resist apoptosis by downregulating caspase-3. *Mech. Ageing Dev.* **125**, 777–783 (2004).
34. Wood, L. D. *et al.* Characterization of ataxia telangiectasia fibroblasts with extended life-span through telomerase expression. *Oncogene* **20**, 278–288 (2001).
35. Ouellette, M. M., McDaniel, L. D., Wright, W. E., Shay, J. W. & Schultz, R. A. The establishment of telomerase-immortalized cell lines representing human chromosome instability syndromes. *Hum. Mol. Genet.* **9**, 403–411 (2000).
36. Lee, K. M., Choi, K. H. & Ouellette, M. M. Use of exogenous hTERT to immortalize primary human cells. *Cytotechnology* **45**, 33–38 (2004).

37. Morales, C. P. *et al.* Absence of cancer-associated changes in human fibroblasts immortalized with telomerase. *Nat. Genet.* **21**, 115 (1999).
38. Jiang, X. R. *et al.* Telomerase expression in human somatic cells does not induce changes associated with a transformed phenotype. *Nat. Genet.* **21**, 111–114 (1999).
39. Young, A. T. L., Lakey, J. R. T. & Moore, R. B. Transient telomerase expression in normal somatic cells leads to telomere extension and increased proliferation in the absence of malignant transformation. *Transplantation* **78**, 108 (2004).
40. hTERT Immortalized Cell Lines. Available at:
https://www.atcc.org/Products/Cells_and_Microorganisms/hTERT_Immortalized_Cell_Lines.aspx. (Accessed: 28th January 2018)
41. Menkes, J. H. & Stein, N. Fibroblast cultures in Huntington's disease. *N. Engl. J. Med.* **288**, 856–857 (1973).
42. Kirk, D., Parrington, J. M., Corney, G. & Bolt, J. M. Anomalous cellular proliferation in vitro associated with Huntington's disease. *Hum. Genet.* **36**, 143–154 (1977).
43. Atwal, R. S. *et al.* Huntingtin has a membrane association signal that can modulate huntingtin aggregation, nuclear entry and toxicity. *Hum. Mol. Genet.* **16**, 2600–2615 (2007).
44. Reis, S. A. *et al.* Striatal neurons expressing full-length mutant huntingtin exhibit decreased N-cadherin and altered neuritogenesis. *Hum. Mol. Genet.* **20**, 2344–2355 (2011).
45. Maiuri, T. *et al.* Huntingtin is a scaffolding protein in the ATM oxidative DNA damage response complex. *Hum. Mol. Genet.* **26**, 395–406 (2017).
46. Milakovic, T. & Johnson, G. V. W. Mitochondrial respiration and ATP production are significantly impaired in striatal cells expressing mutant huntingtin. *J. Biol. Chem.* **280**,

30773–30782 (2005).

47. Acuña, A. I. *et al.* A failure in energy metabolism and antioxidant uptake precede symptoms of Huntington's disease in mice. *Nat. Commun.* **4**, 2917 (2013).
48. Gu, X. *et al.* Serines 13 and 16 are critical determinants of full-length human mutant huntingtin induced disease pathogenesis in HD mice. *Neuron* **64**, 828–840 (2009).
49. Atwal, R. S. *et al.* Kinase inhibitors modulate huntingtin cell localization and toxicity. *Nat. Chem. Biol.* **7**, 453–460 (2011).
50. Di Pardo, A. *et al.* Ganglioside GM1 induces phosphorylation of mutant huntingtin and restores normal motor behavior in Huntington disease mice. *Proc. Natl. Acad. Sci. U. S. A.* **109**, 3528–3533 (2012).
51. DiGiovanni, L. F., Mocle, A. J., Xia, J. & Truant, R. Huntingtin N17 domain is a reactive oxygen species sensor regulating huntingtin phosphorylation and localization. *Hum. Mol. Genet.* **25**, 3937–3945 (2016).
52. Genetic Modifiers of Huntington's Disease (GeM-HD) Consortium. Identification of Genetic Factors that Modify Clinical Onset of Huntington's Disease. *Cell* **162**, 516–526 (2015).
53. Smith, M. L., Chen, I. T., Zhan, Q., O'Connor, P. M. & Fornace, A. J., Jr. Involvement of the p53 tumor suppressor in repair of u.v.-type DNA damage. *Oncogene* **10**, 1053–1059 (1995).
54. Liu, Y. & Kulesz-Martin, M. p53 protein at the hub of cellular DNA damage response pathways through sequence-specific and non-sequence-specific DNA binding. *Carcinogenesis* **22**, 851–860 (2001).
55. Fritsche, M., Haessler, C. & Brandner, G. Induction of nuclear accumulation of the tumor-suppressor protein p53 by DNA-damaging agents. *Oncogene* **8**, 307–318 (1993).

56. Feng, Z. *et al.* p53 tumor suppressor protein regulates the levels of huntingtin gene expression. *Oncogene* **25**, 1–7 (2006).
57. Bae, B.-I. *et al.* p53 mediates cellular dysfunction and behavioral abnormalities in Huntington's disease. *Neuron* **47**, 29–41 (2005).
58. Bodnar, A. G. *et al.* Extension of life-span by introduction of telomerase into normal human cells. *Science* **279**, 349–352 (1998).
59. Vaziri, H. & Benchimol, S. Reconstitution of telomerase activity in normal human cells leads to elongation of telomeres and extended replicative life span. *Curr. Biol.* **8**, 279–282 (1998).
60. Potapova, T. A., Zhu, J. & Li, R. Aneuploidy and chromosomal instability: a vicious cycle driving cellular evolution and cancer genome chaos. *Cancer Metastasis Rev.* **32**, 377–389 (2013).
61. Dürbaum, M. & Storchová, Z. Effects of aneuploidy on gene expression: implications for cancer. *FEBS J.* **283**, 791–802 (2016).
62. Keum, J. W. *et al.* The HTT CAG-Expansion Mutation Determines Age at Death but Not Disease Duration in Huntington Disease. *Am. J. Hum. Genet.* **98**, 287–298 (2016).
63. Warner, J. P., Barron, L. H. & Brock, D. J. A new polymerase chain reaction (PCR) assay for the trinucleotide repeat that is unstable and expanded on Huntington's disease chromosomes. *Mol. Cell. Probes* **7**, 235–239 (1993).
64. Walen, K. H. Human diploid fibroblast cells in senescence; cycling through polyploidy to mitotic cells. *In Vitro Cell. Dev. Biol. Anim.* **42**, 216–224 (2006).
65. Debacq-Chainiaux, F., Erusalimsky, J. D., Campisi, J. & Toussaint, O. Protocols to detect senescence-associated beta-galactosidase (SA- β gal) activity, a biomarker of senescent cells in

- culture and in vivo. *Nat. Protoc.* **4**, 1798 (2009).
66. Lemons, J. M. S. *et al.* Quiescent fibroblasts exhibit high metabolic activity. *PLoS Biol.* **8**, e1000514 (2010).
67. Küppers, M., Ittrich, C., Faust, D. & Dietrich, C. The transcriptional programme of contact-inhibition. *J. Cell. Biochem.* **110**, 1234–1243 (2010).
68. Goldstein, S. & Singal, D. P. Senescence of cultured human fibroblasts: mitotic versus metabolic time. *Exp. Cell Res.* **88**, 359–364 (1974).
69. Schwarzacher, H. G. & Schnedl, W. Endoduplication in human fibroblast cultures. *Cytogenetics* **4**, 1–18 (1965).
70. Munsie, L. N., Desmond, C. R. & Truant, R. Cofilin nuclear–cytoplasmic shuttling affects cofilin–actin rod formation during stress. *J. Cell Sci.* (2012).
71. Muchowski, P. J., Ning, K., D’Souza-Schorey, C. & Fields, S. Requirement of an intact microtubule cytoskeleton for aggregation and inclusion body formation by a mutant huntingtin fragment. *Proc. Natl. Acad. Sci. U. S. A.* **99**, 727–732 (2002).
72. Hoffner, G., Kahlem, P. & Djian, P. Perinuclear localization of huntingtin as a consequence of its binding to microtubules through an interaction with beta-tubulin: relevance to Huntington’s disease. *J. Cell Sci.* **115**, 941–948 (2002).
73. Folch, J. *et al.* Role of cell cycle re-entry in neurons: a common apoptotic mechanism of neuronal cell death. *Neurotox. Res.* **22**, 195–207 (2012).
74. Lu, M., Boschetti, C. & Tunnacliffe, A. Long Term Aggresome Accumulation Leads to DNA Damage, p53-dependent Cell Cycle Arrest, and Steric Interference in Mitosis. *J. Biol. Chem.* **290**, 27986–28000 (2015).

75. Nath, S., Munsie, L. N. & Truant, R. A huntingtin-mediated fast stress response halting endosomal trafficking is defective in Huntington's disease. *Hum. Mol. Genet.* **24**, 450–462 (2015).
76. Landles, C., Weiss, A., Franklin, S., Howland, D. & Bates, G. Caspase-6 does not contribute to the proteolysis of mutant huntingtin in the HdhQ150 knock-in mouse model of Huntington's disease. *PLoS Curr.* **4**, e4fd085bfc9973 (2012).
77. Sapp, E. *et al.* Native mutant huntingtin in human brain: evidence for prevalence of full-length monomer. *J. Biol. Chem.* **287**, 13487–13499 (2012).
78. Atwal, R. S. & Truant, R. A stress sensitive ER membrane-association domain in Huntingtin protein defines a potential role for Huntingtin in the regulation of autophagy. *Autophagy* **4**, 91–93 (2008).
79. Vidal, R. L. *et al.* Targeting the UPR transcription factor XBP1 protects against Huntington's disease through the regulation of FoxO1 and autophagy. *Hum. Mol. Genet.* **21**, 2245–2262 (2012).
80. Maiuri, T., Woloshansky, T., Xia, J. & Truant, R. The huntingtin N17 domain is a multifunctional CRM1 and Ran-dependent nuclear and ciliary export signal. *Hum. Mol. Genet.* **22**, 1383–1394 (2013).
81. Hall, L. L., Smith, K. P., Byron, M. & Lawrence, J. B. Molecular anatomy of a speckle. *Anat. Rec. A Discov. Mol. Cell. Evol. Biol.* **288**, 664–675 (2006).
82. Campalans, A., Amouroux, R., Bravard, A., Epe, B. & Radicella, J. P. UVA irradiation induces relocalisation of the DNA repair protein hOGG1 to nuclear speckles. *J. Cell Sci.* **120**, 23–32 (2007).

83. Lin, S., Coutinho-Mansfield, G., Wang, D., Pandit, S. & Fu, X.-D. The splicing factor SC35 has an active role in transcriptional elongation. *Nat. Struct. Mol. Biol.* **15**, 819–826 (2008).
84. Munsie, L. *et al.* Mutant huntingtin causes defective actin remodeling during stress: defining a new role for transglutaminase 2 in neurodegenerative disease. *Hum. Mol. Genet.* **20**, 1937–1951 (2011).
85. Wang, S. & El-Deiry, W. S. p53, cell cycle arrest and apoptosis. in *25 Years of p53 Research* 141–163 (Springer, 2007).
86. Shaw, P. H. The role of p53 in cell cycle regulation. *Pathol. Res. Pract.* **192**, 669–675 (1996).
87. Reinhardt, H. C. & Schumacher, B. The p53 network: cellular and systemic DNA damage responses in aging and cancer. *Trends Genet.* **28**, 128–136 (2012).

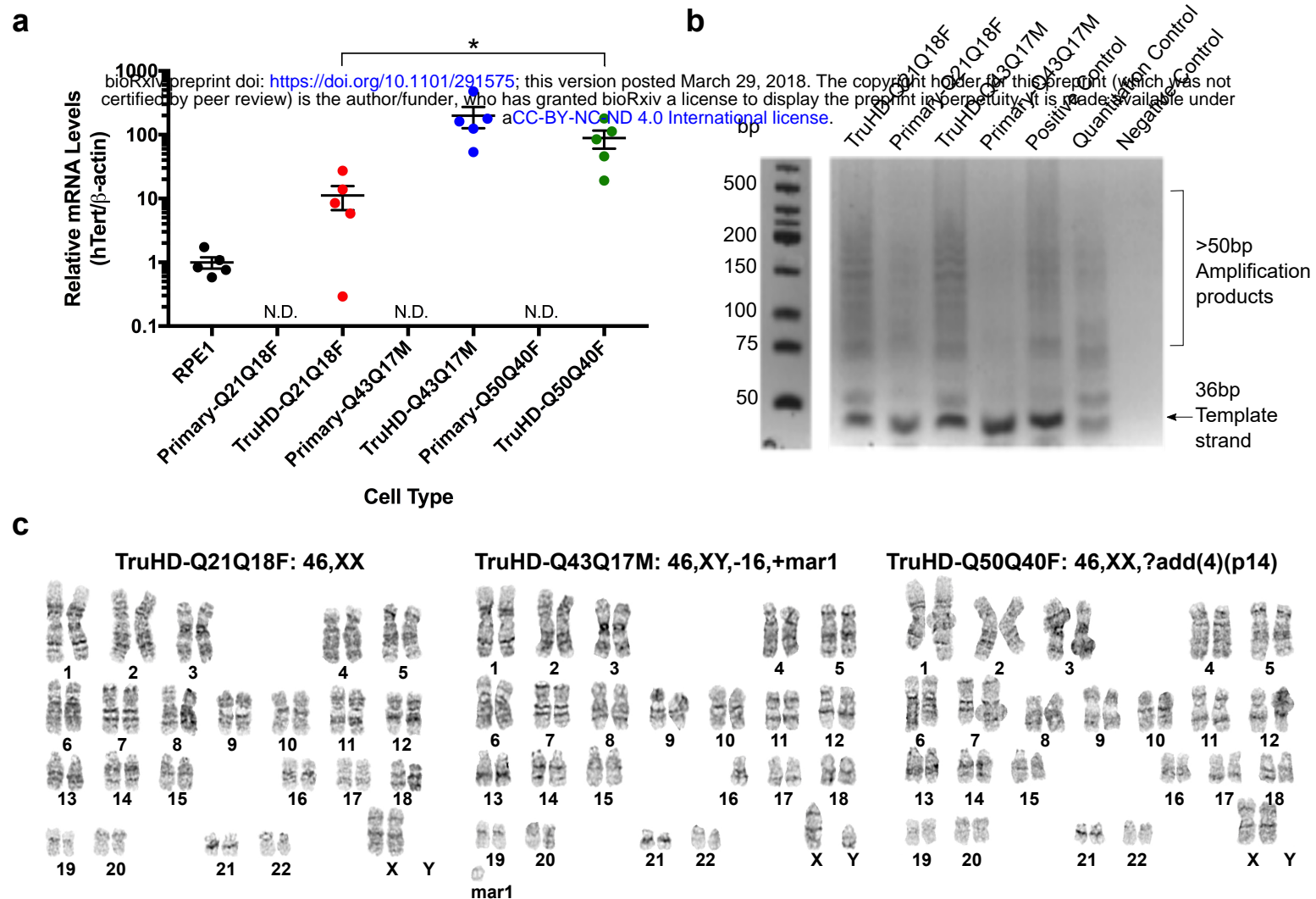


Figure 1

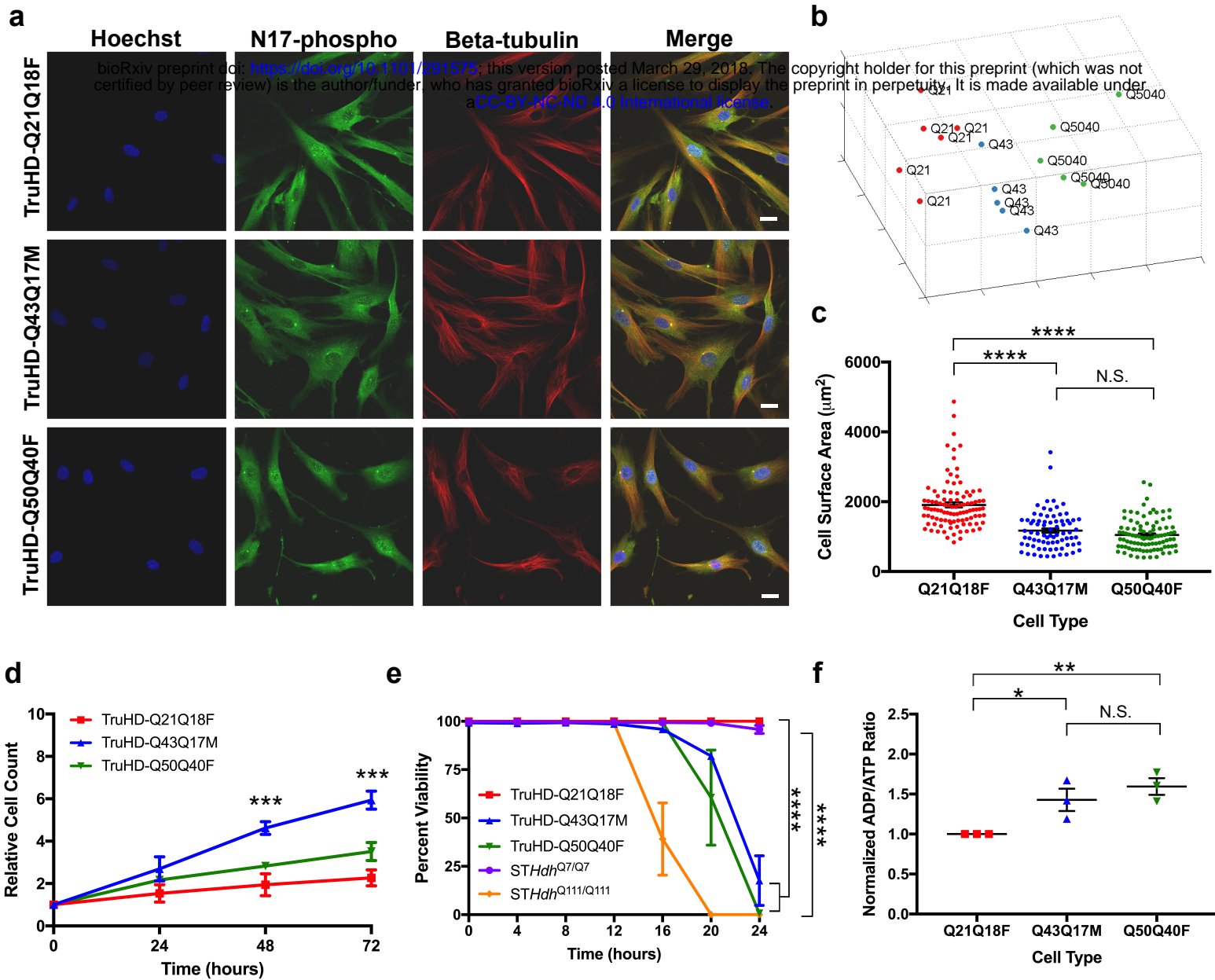


Figure 2

a

bioRxiv preprint doi: <https://doi.org/10.1101/291575>; this version posted March 29, 2018. The copyright holder for this preprint (which was not certified by peer review) is the author/funder, who has granted bioRxiv a license to display the preprint in perpetuity. It is made available under aCC-BY-NC-ND 4.0 International license.

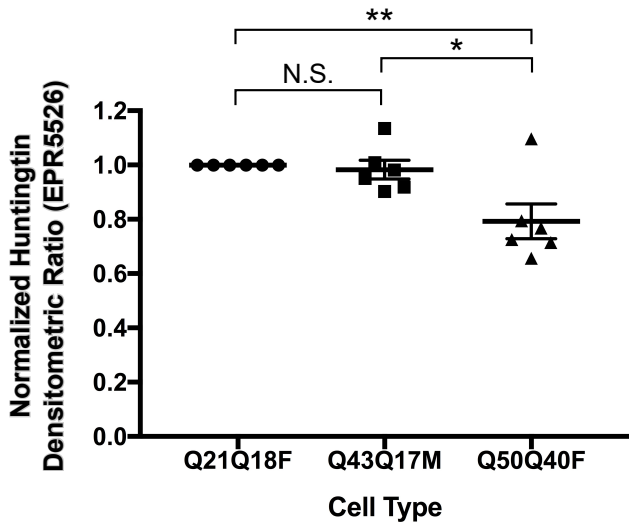
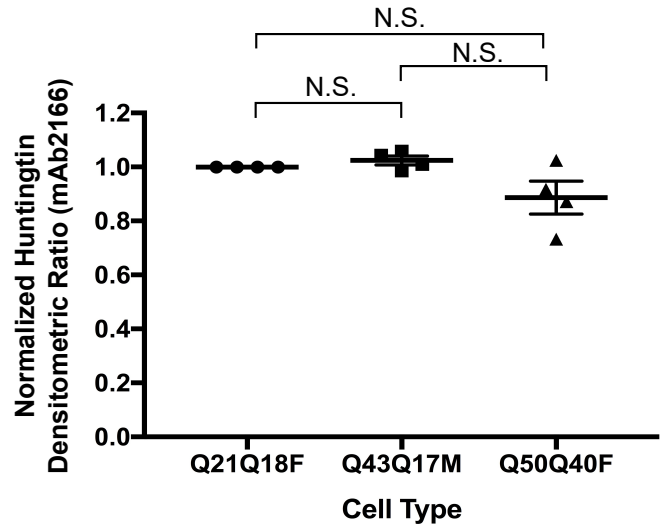
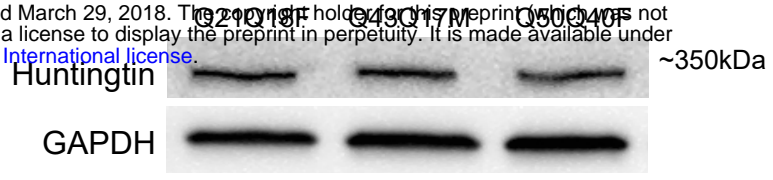
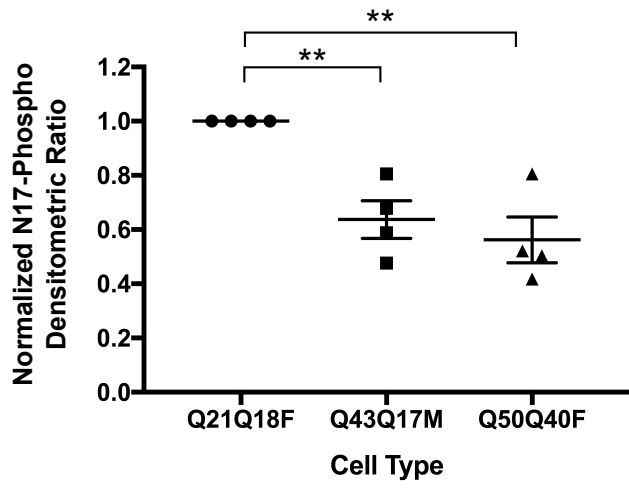
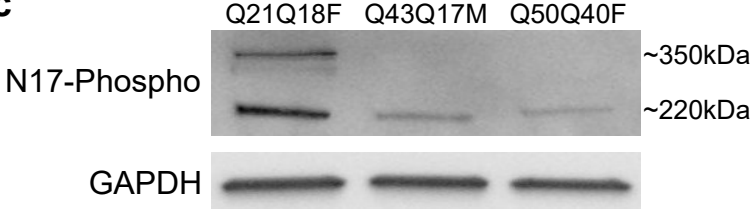
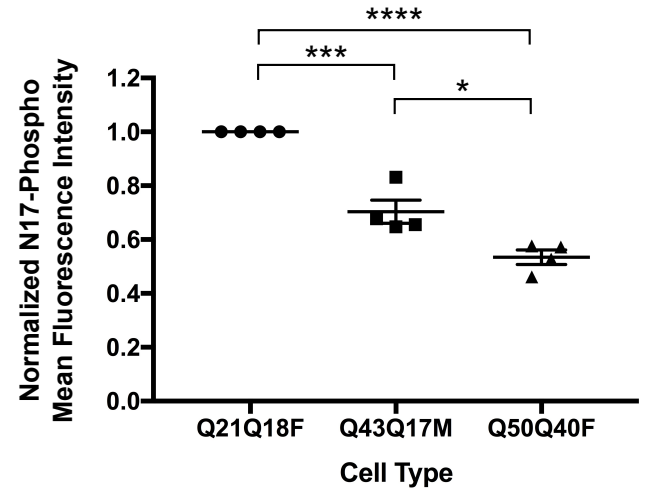
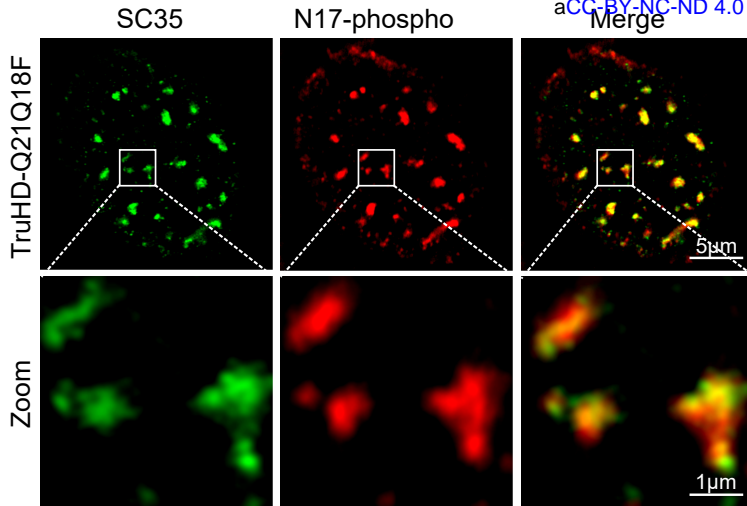
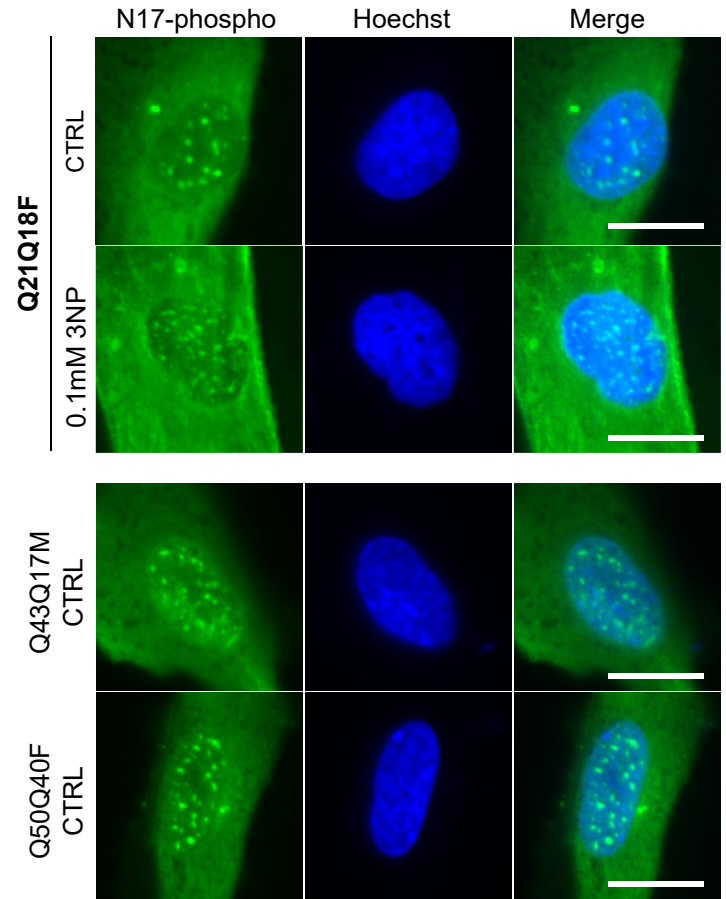
**b****c****d**

Figure 3

a



b



c

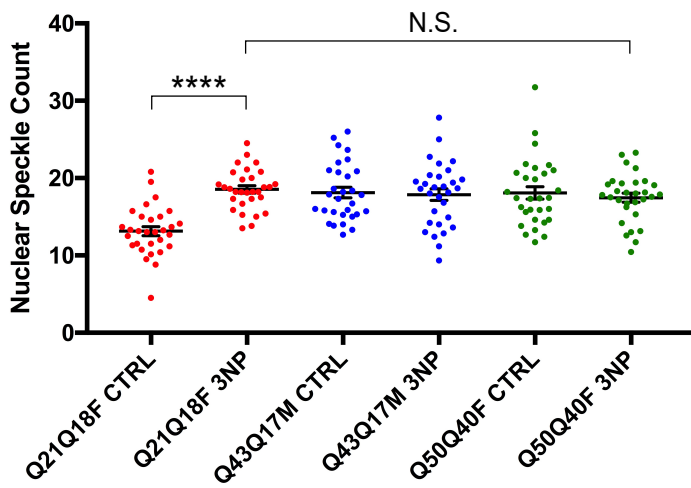


Figure 4